ACS APPLIED MATERIALS & INTERFACES

Research Article

www.acsami.org

Mesosponge Optical Sinks for Multifunctional Mercury Ion Assessment and Recovery from Water Sources

Sherif A. El-Safty,*[,†,‡] Masaru Sakai,[§] Mahmoud M. Selim,[∥] and Awatif A. Hendi[⊥]

[†]National Institute for Materials Science (NIMS), 1-2-1 Sengen, Tsukuba-shi, Ibaraki-ken, 05-0047, Japan

[‡]Graduate School for Advanced Science and Engineering, Waseda University, 3-4-1 Okubo, Shinjuku-ku, Tokyo, 169-8555, Japan

[§]Centre for Research in Isotopes & Environmental Dynamics, Tsukuba University, 265-38 Shin Makita, Tsukuba-shi, Ibaraki 305-0076, Japan

[∥]Department of Mathematics, Al-Aflaj College of Science and Human Studies, Prince Sattam Bin Abdulaziz University, Al-Aflaj 710-11912, Saudi Arabia

[⊥]Department of Physics, College of Science and Humanities−Hawtat Bani Tamim, Prince Sattam Bin Abdulaziz University, Hawtat Bani Tamim, Saudi Arabia

Supporting Information

ABSTRACT: Using the newly developed organic−inorganic colorant membrane is an attractive approach for the optical detection, selective screening and removal, and waste management recovery of highly toxic elements, such as Hg(II) ions, from water sources. In the systematic mesosponge optical sinks (MOSs), anchoring organic colorants into 3D, well-defined cage cavities and interconnected tubular pores (10 nm) in the long microscale channels of membrane scaffolds enhances the requirements and intrinsic properties of the hierarchal membrane. This scalable design is the first to allow control of the multifunctional processes of a membrane in a one-step screening procedure, such as the detection/recognition, removal, and filtration of ultratrace Hg(II) ions, even from actual water sources (i.e., tap, underground). The selective recovery, detection, and extraction processes of Hg(II) ions in a heterogeneous mixture with inorganic cations and anions as well as organic molecules and surfactants are mainly dependent on the structure of the colorant agent, the pH conditions, competitive ion-system compositions and concentrations, and Hg-to-colorant binding events. Our result shows that the solid MOS membrane arrays can be repeatedly recycled and retain their hierarchal mesosponge sink character, avoiding fouling via the precipitation of metal salts as a result of the reuse cycle. The Hg(II) ion rejection and the permeation of nonselective elements based on the membrane filtration protocol may be key considerations in water purification and separation requirements. The selective recovery process of Hg(II) ions in actual contaminated samples collected from tap and underground water sources in Saudi Arabia indicates the practical feasibility of our designed MOS membrane arrays.

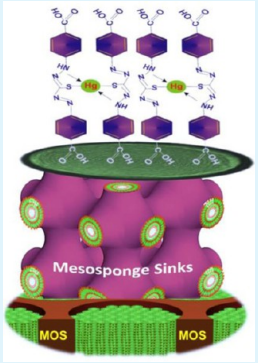

KEYWORDS: *mercury, water sources, sinks, mesosponge, optical, sensor, filter, recovery*

1. INTRODUCTION

Several porous membranes have been recently used as anisotropic hard templates to control the orientation and textural features of nanomaterials based on self-assembly, thermal evaporation, or electrochemical deposition techniques within the confined channels of porous membranes.[1,2] Porous anodic alumina membrane (AAM) has been reported as one of the best hard templates because of its easy electrochemical fabrication process, controllable pore diameter and depth, cylindrical shape, periodicity, well-ordered structure, mechanically and thermally stable vertically parallel pore structures, and low permeation resistance.[3] Thus, AAMs have been widely used as templates to fabricate various nanostructured materials (such as dots, tubes, fibers, rods, and wires) with a controlled diameter and aspect ratio.[4,5] In 2009, Han et al. reported on various silica-based organic−inorganic hybrid nanotubes (NTs) as chromogenic sensors for different heavy metal ions.[6,7] Silica NTs exhibit fluorescence selectivity that is approximately 3-fold higher than that of silica nanoparticles (NPs) because of their lower immobilized chelator content. Thus, silica NT-like morphology has great potential in the design of chemical optical sensors.[8]

AAMs have been used as templates to fabricate hierarchically structured silica materials inside AAM channels to form silica nanowires, nanofibers, and NTs based on different deposition techniques.[9−14] Combining periodic mesoporous silica systems with porous AAM hosts can improve the efficiency of mesoporous materials and lead to the design of novel mesofilter systems for environmental cleanup systems and chemical sensors. Different morphologies of silica NTs (S-helix, core−shell triple helix, core−shell D-helix, and so on) were synthesized on the basis of the dimensions of AAM

Received: December 29, 2014
Accepted: May 12, 2015
Published: May 12, 2015

DOI: 10.1021/acsami.5b02969
ACS Appl. Mater. Interfaces 2015, 7, 13217−13231

nanochannels (pore diameter and depth) to physically confine a suitable precursor solution and surfactant template.[1−5] In 2004, Martin and Siwy reported the fabrication of a hybrid composite membrane that consists of mesoporous silica confined within AAM channels as pores within pores; this membrane is a promising candidate for size-exclusive molecular filter systems.[15] We recently fabricated nanostrands inside AAM channels as size-selective filters for the ultrafine filtration of noble metal NPs and proteins with a large molecular size while a hefty amount of retentate was generated. Thus, the design of mesofilter membranes with mesocage pores that are perpendicular to the longitudinal axis of the nanochannels and uniformly multidirectional nanoscale pores will effectively enhance separation techniques for nanosized hazardous pathogens and viruses.[15] To broaden the application of mesoporous hybrid AAMs, smart sensor/captor/filter devices based on AAMs are essential for environmental monitoring and green chemistry; such devices are necessary even in basic laboratory assays for controlled multifunction processes in the one-step screening (such as selective removal, sensing, visualization, filtration, and recovery) of hazardous and pathogenic species from water sources.

Mercury (Hg) is a highly toxic (>1 ppb), carcinogenic, and nonbiodegradable element[16] that is widely released into the environment, particularly in industrial areas such as gold production plants, coal plants, and manufacturers of thermometers, barometers, caustic soda, and Hg lamps. Hg exists in various forms and has extremely harmful effects on the nervous, immune, and digestive systems, as well as on the skin, lungs, kidneys, and eyes, even in trace amounts.[16,17] Furthermore, the adverse health effects of Hg are not only related to the Hg ions and to doses, but also to sampling exposure time. Long periods of exposure to Hg vapor can cause brain injury and, eventually, death. Hg compounds are extremely toxic to fetuses and infants. Exposure of pregnant women to Hg has occasionally led to serious defects in their unborn children.[18] Hg is emitted from industrial and natural activities, transmitted effectively through plants and other aquatic sources, and bioconcentrated in the food chain. In humans, approximately 80% of inhaled Hg vapor is captivated via the respiratory tract system; however, Hg also enters the circulatory blood system and is distributed throughout the entire body. Continuing exposure by inhalation, even at the ultratrace range of 0.7−42 $\mu g/m^3$, has been proven to cause sleep disturbance, muscle disorders, and impaired mental skills. When they disperse in the environment, Hg(II) ions undergo a series of biogeochemical transformations into toxic chemical species. This phenomenon has motivated intensive research on the biological effects of such ions on humans.[18,19] The acute toxicity thresholds of Hg(II) ions in freshwater creatures differ from 5−230 $\mu g/L$ in shellfishes to approximately 60−800 $\mu g/L$ in fish. Controlled assessment methods that can improve diagnostics in medical applications, health and safety, and security remain an attractive approach to analyze current ultratrace levels of Hg(II) ion toxicity.[16−20] Moreover, toxic Hg(II) ions entering into rivers and soil as a result of exploitation, abuse, and smelting may progressively accumulate in humans after they become elaborated via bioactivities; as such, trace detection of Hg(II) ions is important.[21−25] Consequently, highly reliable, sustainable, easy-to-use, low-cost, and sensitive designs are necessary. Advances in technology have provided analytical methods that are capable of recognition and quantitation of trace Hg(II) ions. Currently available sensing methods that are capable of quantifying traces of heavy metals at low concentrations include atomic absorption spectroscopy and inductively coupled plasma (ICP) combined with mass spectrometry (ICP−MS) or atomic emission spectrometry (ICP−AES).[21−25] ICP−MS is considered a powerful method because of its sensitivity and multicomponent functionalities. Other devices, such as electrochemical techniques, flame atomic fluorescence spectrometry, molecular absorption spectrometry, neutron activation, and X-ray fluorescence, have also been developed. Most of these methods have provided analytical devices and assays that can detect and quantify trace concentrations of Hg species. However, the majority of these methods are normally restricted to wealthy institutions, organizations, and pollution-monitoring agencies in developing countries. In addition, careful planning and several handling steps during sample preparation and standardization are frequently required in these analytical methods. Therefore, new or improved, easy-to-use, and sustainable commercial indicators for household use are in demand.[25−31] Important developments of optical chemical sensors for Hg(II) ion detection and recognition using proteins, fluorophores, chromophores, and polymers have been reported.[32−35] Though these sensing designs are certainly valuable and have individual advantages, it cannot be denied that they have some demerits.[6,7,36−42] Given the limitations in associating Hg(II) ion sensing and visual capture with unexpected functionality in selectivity and sensitive visualization and detection below the permissible level of toxic ions, the demand to develop low-cost, mass-scale optical chemical sensors and adsorbents for the precise recovery, quick detection, and selective recognition and monitoring of contaminant species with limited sensitivity for detecting below the tolerable level of toxic Hg(II) ions in water sources is increasing worldwide, particularly in countries with serious water scarcity issues and shortage of safe drinking water.

Recent efforts involve fabricating mesoporous optical chemical sensors that incorporate simple fabrication techniques and mass-scale materials with optimization toward commercialization.[39−47] However, the following key components that can help provide a prospective optical nanosensor/captor/filter for a controlled environmental cleanup system remain to be addressed: (1) Multifunctional processes must be controlled in complete water purification systems, such as sensing/removal and separation in a one-step screening procedure. (2) There must be selective target contamination among high concentrations of interfered and competitive mixture species. For example, the selective separation of Hg(II) ions from divalent cations such as Cd(II), Pb(II), Mn(II), Cu(II), Co(II), and Fe(II) is difficult; the hydrated forms of these ions are similar in size and exhibit similar charges. (3) The arrangement of real water system modules should be integrated into various process configurations, such as the detection/removal of ultratrace concentrations in water sources (tap, underground, wastewater, and seawater). However, no single-sensing class or technology that can effectively detect Hg(II) ions in all forms of water sources is yet available. (4) In miniature analytical instruments, a batch process is used to improve sensor performance in terms of the sensitivity of detectors and sampling systems, as well as the separation or preconcentration of Hg(II) ions using several methods.

In the present study, membrane arrays of mesosponge optical sinks (MOSs) were fabricated directly on densely surface-decorated inorganic−organic active layers that are well-aligned

DOI: 10.1021/acsami.5b02969
ACS Appl. Mater. Interfaces 2015, 7, 13217−13231

in a perpendicular direction into the open-end NT pores of hybrid AAM channels. To our knowledge, no approach for optical chemical sensor/captor/filter spongelike arrays of Hg(II) ions based on ordered mesocage cavitylike sinks entirely filling the uniform NT hybrid microscale channels has yet been reported. The synthetic protocol creates spherical mesocage pores with multidirectional nanoscale windows, which are vertical to the longitudinal long-axis of the functional AAM channel gradients. This protocol will effectually enhance the accessibility, adsorptive capacity, and stabilization of the dense decoration dressing process of a wide range of hydrophilic colorants, which leads to the potential formation of MOSs. Membrane analysis methods based on a flow-through module cell detector and benchtop contact techniques demonstrate a simple one-step sensing/capture/recovery process to quantify and visually detect Hg(II) ions as well as to filter other metal components (Scheme 1). This systematic design also exhibits

Scheme 1. Systematic Fabrication Design of MOSs through Trifunctional, Dense Decoration of Mesocage Silica NTs by Colorants (L1, L2, and L3) for the Hg(II) Ion Sensing/Removal/Separation/Recovery Processes, Membrane Stability after Hg(II) Ion Collecting, and Filtration To Give Water Free of Hg(II) Ions[a]

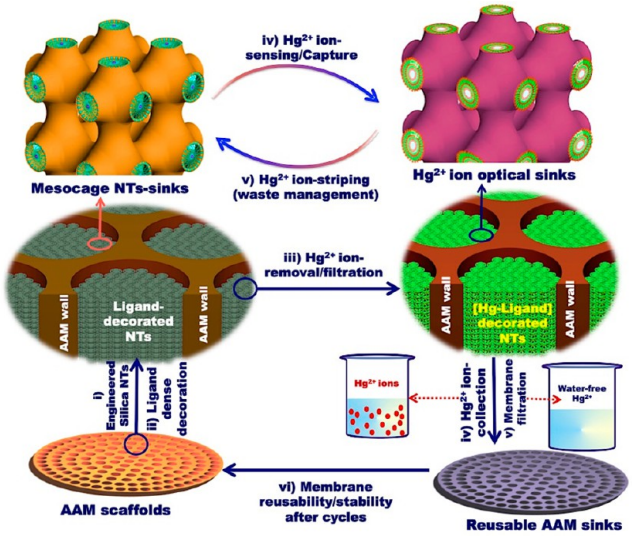

[a]The top scheme shows evidence of the reversible, optical sensing functionality during the capture of Hg(II) ions into MOSs.

long-standing signaling functionalities over a wide solution pH range (i.e., 4.0−11.0) that provide sensitive visualization, selectivity, and reusability while fast kinetic detection/removal/filtration of Hg(II) ions in different water sources is maintained. The simple recovery of Hg(II) ions from actual contaminated environmental samples, which were collected from tap and underground water sources in Abha City, Saudi Arabia, was achieved. Our finding indicates that the MOSs can be potential candidate materials for hazard remediation and waste control of water sources.

2. EXPERIMENTAL SECTION

2.1. Chemicals. All materials were used as produced without further purification. Triblock poly(ethylene oxide)-poly(propylene oxide)-poly(ethylene oxide) copolymers of Pluronic F108 ($PEO_{100}PPO_{70}PEO_{100}$) and tetramethylorthosilicate (TMOS), which was used as the silica source, *N*-trimethoxysilylpropyl-*N*,*N*,*N*-trimethylammonium chloride (TMAC), and dilauryldimethylammonium bromide (DDAB) were obtained from Sigma-Aldrich Co. Ltd. The solvents dodecane ($C_{12}H_{26}$) and anhydrous toluene (C_7H_8) were obtained from Wako Company Ltd. (Osaka, Japan). AAM with a pore size of 200 nm, a diameter of 2.5 cm, and a thickness of 60 μm was purchased from Whatman, Co. Ltd. Mercury chloride ($HgCl_2$) and other metal ion standard solutions were obtained from Wako Company Ltd. The commercially available pyrogallosulfonphthalein (**L1**) and 3,3′-bis[*N*,*N*-bis(carboxymethyl)aminomethyl]-*o*-cresolsulfonephthalein tetrasodium salt (**L2**) were purchased from Sigma-Aldrich. In addition, dicarboxylate 1,5-diphenylthiocarbazone (**L3**) probe was prepared as we recently reported.[40] The working conditions of MOSs membranes were optimized by benchtop filtration or flow-through module cell detector techniques. When applying the benchtop method, the fixed membrane sensor (macroscopic scale disk) was spiked with a buffered Hg(II) ion analyte solution of 20 mL. The Hg(II) and other metal ion concentrations were determined by using ICP−MS.

2.2. Fabrication of MOS Membrane. The MOS arrays were successfully fabricated by three consecutive steps (Scheme 1). First, the grafting of solid AAM carrier with a surface modifier such as a silane coupling agent (i.e., TMAC) occurred. Under typical grafting conditions, a mixture of TMAC and anhydrous toluene was added into AAM and thoroughly refluxed in a Soxhlet apparatus for 12 h under N_2 at 25 °C. The TMAC/AAM was gently sealed in a container, washed with ethanol to remove the unreacted TMAC, and then dried in an oven at 60 °C. Second, 3D mesocage NT hybrid AAM channels were formed via pressure-assisted templating of the microemulsion mesophase of copolymer Pluronic F108 (F108). In typical synthesis protocol, a homogeneous solution of 1.4 g of F108, 10−20 g of ethanol, 2 g of TMOS, and 1.25 g of H_2O−HCl (pH 1.3) was added dropwise to the TMAC/AAM mixture, and stirring was continued at 45 °C for 10 min. The charged TMAC/AAM was set in a benchtop filtration apparatus and the homogeneous precursor was dropped onto the organic−inorganic TMAC/AAM layer membrane. The pressure-driven penetration of the precursor solutions (F108/TMOS/alkane/H_2O) into TMAC/AAM channels was carried out under vacuum with a starting pressure of 50 kPa. To ensure the complete filling of mesoporous silica into the AAM channels, the penetration method of the precursor solutions was repeatedly carried out. The as-synthesized AAM−TMAC−silica/F108 mesophase structures were dried in a sealed container for 10 h at 45 °C. A mixture of ethanol/HCl solution was used to remove the F108 surfactant to avoid the distortion of the organic−inorganic tubular architectures (AAM−TMAC−silica NTs) upon calcination, as evident from ^{29}Si magic-angle spinning nuclear magnetic spectroscopy (see the Supporting Information, section S1, Figure S1 and Scheme 1). Third, the membranes of MOSs (S1, S3, and S2) were synthesized through direct and linker-mediated immobilization of ligands **L1**, **L3**, and **L2** into mesocage NTs hybrid AAM. In the design of S1 and S3, a 100 mL ethanol solution containing approximately 20 mg of **L1** or **L3** was directly dropped into AAM−TMAC−silica NTs and allowed to stand for 20 min, and then the pressure-assisted immobilization of **L1** or **L3** into all the NTs was accomplished at a pressure of 50 kPa. Furthermore, the MOS S3 was fabricated in two steps. First, the linker-mediated synthesis was used to create an active surface site on the AAM−TMAC−silica NTs channels. Thus, a 0.1 M ethanol solution of DDAB was dropped onto the AAM−TMAC−silica NTs membrane under a pressure of 50 kPa. Second, 20 mg of ligand **L2** in water was incorporated with the AAM−TMAC−silica NTs−DDAB membrane. In both steps, pressure-assisted immobilization of DDAB and L3 into the NTs was achieved at a pressure of 50 kPa. In general, the immobilization process was thoroughly repeated to ensure the complete saturation of the organic ligands **L1**, **L2**, and **L3**, as evidenced from the determination of the reflectance signaling spectra. The resulting MOSs S1, S2, and S3 were then dried at 65−70 °C for 3−4 h and then used for recognition/detection/removal/filtration assays of Hg(II) ions (Scheme 1). The amount of immobilized **L1**, **L2**, and **L3** ligand was 0.14, 0.31, and 0.29 mmol/g, respectively.

DOI: 10.1021/acsami.5b02969
ACS Appl. Mater. Interfaces 2015, 7, 13217−13231

2.3. Optical Hg(II) Ion MOSs for Controlled Sensing Functionality. For the precision control of the MOSs membrane sensing functionality and efficiency, target Hg(II) ions were optically monitored using a flow-through module cell detector technique (see the Supporting Information, section S1). In this technique, the optical intensity and color signaling of the solid MOS membrane was identified using a UV−vis spectrometer (CIMPS-Abs-UV). This technique enabled remarkable reflectance spectra response isolations and color changes visible to the human eye even at ultratrace concentrations of Hg(II) analyte (Scheme 1). The standardization/calibration analysis of this detection/recognition method using the flow-through module cell detector technique during Hg(II) ion sensing was measured and repeated ≥10 times. The quantitative analyses were carried out in the range of 2.49×10^{-9} to 9.96×10^{-6} M concentration at optimum sensing conditions. The limit of detection (LOD) of Hg(II) ion sensing by using solid-disk MOSs was estimated from the linear portion of the standardization plot according to the equation LOD = $3\Phi/\omega$, where ω and Φ are the slope and the standard deviation of the graph. To determine the Hg(II) ion capture into the MOSs (S1, S2, and S3) during the sensing efficiency, the cell detector was conducted to the inductively coupled plasma mass spectrometer to measure the rejected solution after complete Hg(II) ion sensing response with a time of 20, 4, and 2 min, respectively (Scheme 2).

Scheme 2. (A) A Benchtop Contact Time Technique for Hg(II) Ion Sensing/Capture Assessment Experiment,[a] (B) MOS Membrane before Use, and (C) MOS Membrane after Uptake of Hg Ions

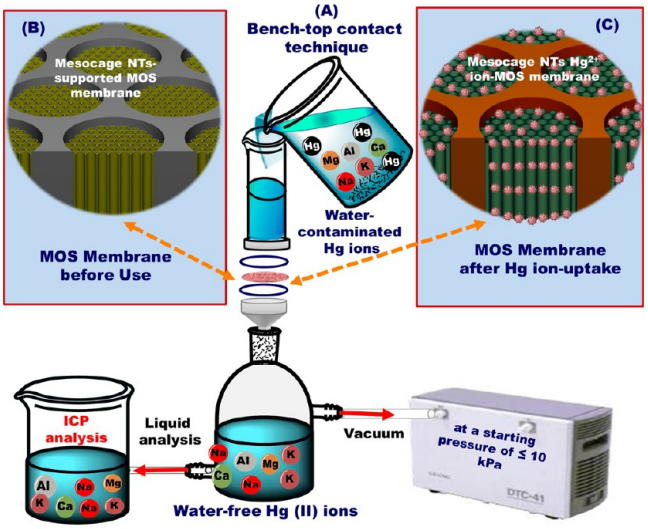

[a]In this technique, the MOS membrane was statically fixed in an ordinary filtration apparatus for the visual detection/recognition, exclusive removal of Hg(II) ion, and filtration of other metal ions in water. The permeated solution (i.e., at the backside) of ions was analyzed by ICP−MS. The color changes of the solid disk of the MOS membrane (C), which indicated the presence of rejected Hg(II) ions, were monitored by UV−vis spectroscopy.

2.4. MOSs for Separation/Filtration/Recovery Assessment of Hg(II) Ions. In a typical Hg(II) ion assessment experiment (Scheme 1), the benchtop contact time technique was used for the visual detection, exclusive separation of Hg(II) ion, and filtration of other metal ions in water. In such a benchtop filtration/separation technique, the MOS (with diameter of 2.5 cm) was fixed in an easy-to-use filtration tool (Scheme 2). A 20 mL portion of a buffered mixture at a solution pH of 4.8, 8, and 10.9 containing Hg(II) and other metal ion concentrations was added to the fixed MOSs (S1, S2 and S3, respectively) membrane model. Afterward (i.e., following the response time of ∼20, 4, and 2 min for S1, S2, and S3, respectively), the solution was filtrated under vacuum at a pressure of 10 kPa at 25 °C. The permeated solution was collected and analyzed by ICP−MS. The color changes of the solid MOS disk, which indicated the presence of rejected Hg(II) ions, were monitored by UV−vis spectroscopy (Schemes 1 and 2). In order to control the optimal experimental conditions, the outlet filtrate (permeated solution) was quantitatively analyzed by using ICP−MS analyses as a function of contact time, pH value, and pressure, respectively. The adsorption capacity of Hg(II) was calculated using the mass balance equation $q = (C_o - C_p)V/m$, where q is the adsorption capacity (mg/g), C_o is the initial Hg(II) concentration (mg/L) of the feed solution, C_p is the permeate concentration (mg/L), V is the volume of the Hg(II) ion bearing solution treated with the MOSs (L), and m is the optical membrane sensor/captor weight (g). Moreover, the rejected Hg(II) ion concentration (C_R, mg/L) on the optical membrane sensor/captor was calculated as follows: $C_R = C_o - C_p$. The adsorption feature and coverage of Hg(II) ions onto the MOS membrane at 25 °C are determined by the Langmuir and Freundlich isotherms.[48,49] The stability constants (log K_s) of the formed [Hg−**L1**], [$(Hg)_2$−**L2**], and [Hg−$(\mathbf{L3})_2$] complexes into the S1, S2, and S3 at pH 4.8, 8, and 10.9 were found to be 2.05, 7.3, and 24.8, respectively, according to the equation log $K_s = [ML]_{Solid}/[L]_{Solid}[M]$, where [M] refers to the concentration of Hg(II) ions in outlet filtrate solution that have not been rejected into MOSs, $[L]_{Solid}$ represents the concentration of free-surface ligand that is not bound to Hg(II) ion, and $[ML]_{Solid}$ denotes the concentration of ligand that is bound to Hg(II) ion.[46]

3. RESULTS AND DISCUSSION

The synthetic design (Scheme 1) of the 3D MOS membrane arrays provides an adequate and stable fabrication process with structural features such as (1) open surfaces as well as condensed and rigid NTs that are vertically aligned along the perpendicular plane of the AAM surfaces; (2) AAM pore channels completely filled with silica NTs as well as **L1**, **L2**, and **L3** colorants; (3) accommodated and oriented **L1**, **L2**, and **L3** probe assemblies in the mesocage ordered patterns that run longitudinally through the NTs; and (4) completely immobilized and decorated colorant moieties in the cubic *Im*3*m* mesocage structure arrangement of the network hybrid channels that run parallel to the AAM wall (see the Supporting Information, sections S2 and S3). These features broaden the applications of the aforementioned optical membrane sensors/captors for toxic Hg(II) ion sensing/capture/filtration processes.

3.1. Architectural Features of MOS Membrane Captor-Based Cubic Cage Silica NTs. The scanning electron microscopy (SEM) images (Figure 1A,B) show the formation of the mesoporous silica NTs within the AAM channels, which indicates perfect impregnation and the presence of densely engineered silica NTs in the AAM. The micrographs revealed well-aligned, open-end NT pores in a direction perpendicular to the AAM channel (Figure 1B). The top view of the SEM image (Figure 1A) indicates the formation of mesoscale cage tubes with open surfaces that completely fill the AAM nanochannels. The SEM images also show that the silica NTs are spatially fixed at a high density in the fabricated structures. The transmission electron microscopy (TEM) micrographs (Figure 1C,D) present the construction of individual mesoporous tubular channels with ordered and hollow spaces that may pass through the longitudinal axis of the silica NTs hybrid channels. A band of ordered mesopore arrays with a specific arrangement and orientation that may be consistent with the dominant body-centered cubic *Im*3*m* geometry being present inside the NTs (Figure 1D), as evidenced from the Fourier transform diffractogram (FTD) pattern (Figure 1E).[50−52] The top view of the HRTEM image (Figure 1F)

DOI: 10.1021/acsami.5b02969
ACS Appl. Mater. Interfaces 2015, 7, 13217−13231

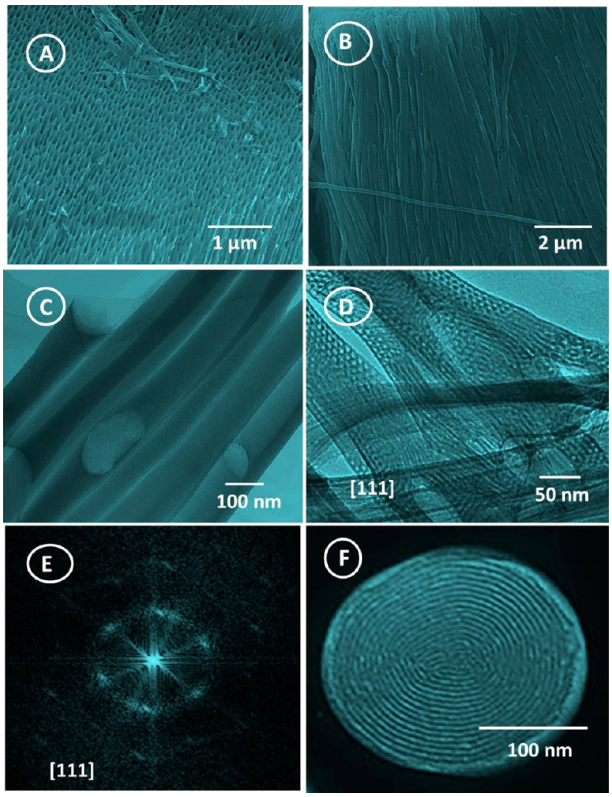

Figure 1. FE-SEM images of MOS recorded along the top view (A) and side view (B). HRTEM patterns with different magnifications (C, D, respectively). (E) FTD pattern of MOS-based mesocage cubic *Im*3*m* geometry recorded along the [111] direction from the TEM image (D). All sets of micrographs (A–D) were recorded after etching of the alumina walls by addition of 5% H_3PO_4 for 24 h at 25 °C. The micrographs (A–D) indicated that the silica NTs clearly showed top–bottom ends with uniform alignment along the perpendicular axis of the AAM channels. (F) The top-view TEM micrograph recorded in the direction perpendicular to MOS S2 hybrid AAM fabricated by using dressing **L2** through the linker agent DDAB.

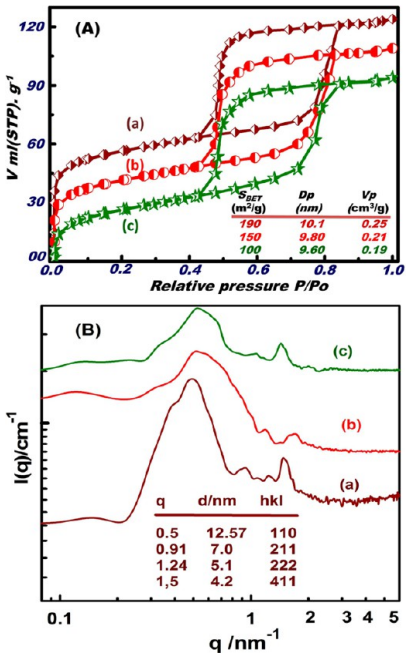

Figure 2. N_2 adsorption/desorption isotherms (A) and SAXS patterns (B) of AAM–TMAC–silica NTs scaffold (a), MOS S1 fabricated by direct dressing with **L1** receptor (b), and S1 after a reuse cycle (c). Insets in part A: surface area (S_{BET}/m^2 g^{-1}), pore volume (V_p/cm^3 g^{-1}), and cage pore cavity (D_p/nm). Inset in part B: assignment of the scattering peaks of AAM–TMAC–silica NTs scaffold (a). The *d*-spacing was calculated from the scattering peak position with $d = 2\pi/q$.

shows that the alumina pores are filled in with the silica–surfactant composite, as indicated by the columnar ordering in all AAM channel vicinities. The top view of the TEM micrograph recorded in the direction perpendicular to the AAM channels indicates that the MOS membrane arrays provide adequate and stable accommodation of the colorants. This phenomenon maintains the specific activity of the molecular probe to effectively capture target ions, as evidenced by the substantial ion-sensing/separation/filtration system functionality (Scheme 1).

The mesoporosity of the cubic *Im*3*m* silica NTs/AAM carrier and cagelike MOS was evaluated using N_2 adsorption/desorption measurements (Figure 2A). The isotherm suggests the fabrication of cagelike pore sinks with spherical cavity (~10.0 nm) and with one size for pore openings (<5 nm), despite the dense decoration of **L1**, **L2**, and **L3** probes into the NTs/AAM channels and the reusability of the AAM sensor. The N_2 isotherm shows type IV mesopore sorption behavior with large type H_2 hysteresis loops; the steepness of the isotherms is well-defined, which indicates large and uniform mesocage structures, as reported previously.[50−52] The synthesis approach provides control over the mesopore size and shape inside the NT hybrid AAM channels. The 3D cage architecture has a high surface area (S_{BET}) and pore volume (V_p) of 190 m^2 g^{-1} and 0.25 cm^3 g^{-1}, respectively. After the immobilization of **L1**, **L2**, and **L3** into the membrane and the capture reusability of Hg(II) ions was established, the surface area was decreased to 150, 100, and 100 m^2 g^{-1}, respectively. The decrease in the textural parameters of the **L1**-, **L2**-, and **L3**-incorporated silica NTs indicates the following findings:

(1) Large amounts of **L1**, **L2**, and **L3** molecules can be immobilized and can become a rigid part of the interior of NTs/AAM channels.

(2) No pore blocking effect of the cage window "pore entrances" was observed as a result of the accommodation and orientation of the **L1**, **L2**, and **L3** probe assemblies in the spherical cavity of the mesocage NTs. This structural integrity may improve MOS workability, in which Hg(II) ions are sensitively detected even at nanomolar concentrations.

(3) The cagelike sink, 3D geometries, and textural features of the MOS membrane are retained even after several reuse cycles.

The small-angle X-ray scattering profile (SAXS) exhibits strong peaks with scattering vector **q** values of 0.5, 0.51, and 0.52 nm, corresponding to the *d*-spacing values of 12.57, 12.3, and 12.1 nm, respectively, which are attributed to the (110) reflection of the silica NTs/AAM carrier; **L1**, **L2**, and **L3** grafted into the NTs/AAM sensor/captor (MOSs); and the reusable sensor/captor, respectively. Scattering peaks within the range of $0.2 < \mathbf{q} < 2.0$ strongly suggest a 3D architecture. Five peaks were revealed in the SAXS pattern assigned to the (110), (200), (211), (222), and (411) scattering planes of the 3D cubic *Im*3*m* structures with a large lattice constant ($a = d_{110}\sqrt{2}$) of 17.8 nm.[5] Furthermore, despite the widening and shift toward the high **q** region in the scattering peaks with **L1**, **L2**, and **L3** loaded in the mesocage cavities or with the ion/sensing and capture processes (Figure 2Bb,c), the resolution

DOI: 10.1021/acsami.5b02969
ACS Appl. Mater. Interfaces 2015, 7, 13217−13231

Scheme 3. Systematic Design of the Chemical Formation of Square Planar [Hg−L1] and [Hg−$(L3)_2$] and Tetrahedral [$(Hg)_2$−L2] Complexes upon the Addition of Hg(II)-Contaminated Water to MOSs S1, S2, and S3 inside the NTs Hybrid Membrane, Respectively[a]

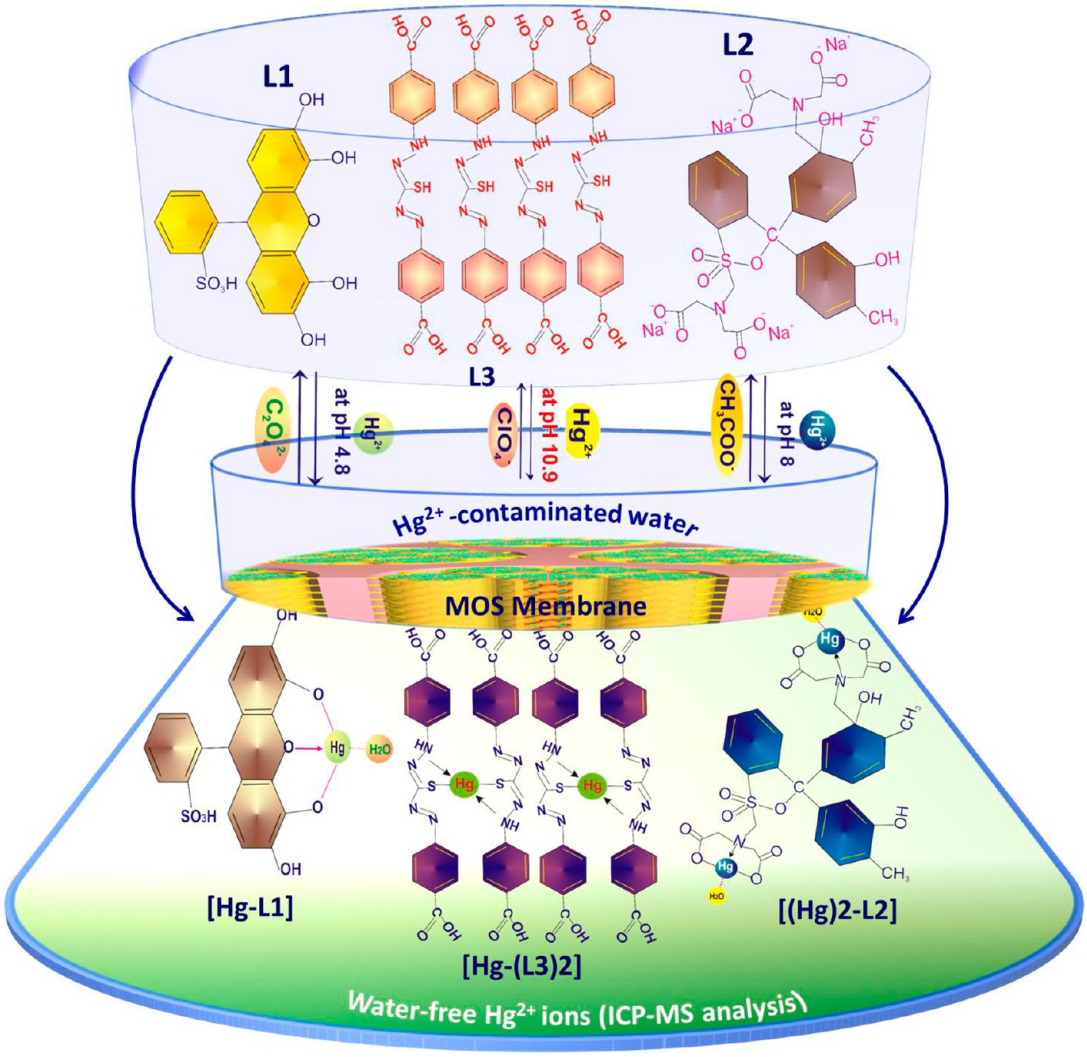

[a]The formation of these complexes indicates the detection/recognition/extraction of metal ions from resources. The reusability of the MOSs was evaluated by examining the sensing/capture efficiency with reuse cycles. The recycling process was carried out by stripping the Hg(II) ion from MOSs surfaces (i.e. decomplexation).

and intensity of these scattering patterns show the retention of 3D mesocages throughout the silica NT hybrid AAM channels.[53] This scattering profile indicates that the **L1**, **L2**, and **L3** colorants are oriented and accommodated by the inner mesocage cavity and pore-opening connectivity. Moreover, these colorants adapt the geometric ordering and atomic structural arrangement of network matrices with crystalline cubic *Im*3*m* symmetry, which gives them great potential as hosts for colorant dyes in MOS sensors/captors/filters.

3.2. Hg(II) Ion Sensing/Removal and Filtration Processes. The pH-dependent sensing/filtration/removal/recovery assays were studied at pH range 1.0−12.5. The Hg^{2+} ion feed concentrations were prepared with different buffer solutions of either 0.01 M sulfuric acid or 0.2 M KCl-HCl and CH_3COOH−CH_3COONa to adjust the pH in the 1−6 range. To help formation of soluble Hg complexes with chlorides and hydroxides in alkaline medium (i.e., Hg(II)−Cl^-−OH^-−H_2O), we used a mixture of 3-morpholinopropanesulfonic acid (MOPS), *N*-cyclohexyl-3-aminopropanesulfonic acid (CAPS), and 2-(cyclohexylamino) ethanesulfonic acid (CHES) to control the pH solution in the 7−12.5 range by using 0.2 M NaOH. In our experimental studies, the standard feed solution of Hg(II) ion was prepared by using $HgCl_2$ salt. We carried out a number of experiments to investigate the effect of the pH range of the feed solution, the concentration of Hg(II) ion, the Hg(II) salt species, and the component composition of feed solutions on the degree of solubility and the mobility of Hg(II) species (see Supporting Information, section S4 and Figures S2−S4).

3.2.1. Hg(II) Ion Sensing Functionality of MOSs. The pH-dependent Hg(II) ion sensing system was optically monitored using a flow-through module cell detector technique. In the experimental assay, the pH value controlled four key features of the optical Hg(II) ion sensor system, namely, (1) visual detection, (2) sensitivity, (3) selectivity, and (4) rapid assessment of Hg(II)-to-receptor reaction kinetics. The AAM−TMAC−NTs layers dressed with **L1**, **L2**, and **L3** receptors/probes have oxygen, sulfur, and nitrogen atoms,

DOI: 10.1021/acsami.5b02969
ACS Appl. Mater. Interfaces 2015, 7, 13217−13231

which can be neutral or protonated, depending on the pH of the feed solution. As a result of a deficiency in the d-orbitals of the Hg(II) ion centers, the [Hg−**L1**], [$(Hg)_2$−**L2**], and [Hg−$(\mathbf{L3})_2$] molecular complexes could be formed at specific pH values of 4.8, 8, and 10.9, respectively (Scheme 3).

A series of optical sensing assays was conducted at a wide-range of pH values with the addition of specific Hg(II) ion concentrations (Figure 3A) to describe the suitable pH

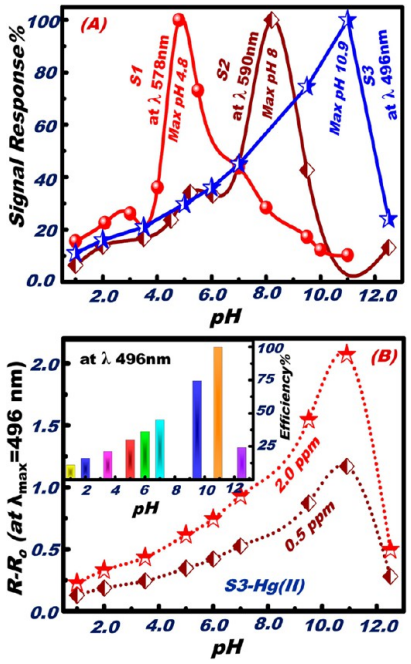

Figure 3. pH-dependent response profiles of the Hg(II) ion−MOSs (S1, S2, and S3). (A) Reflectance signaling responses (%) obtained at λ_{max} = 578, 590, and 496 nm and at a Hg(II) ion concentration of 1 ppm with a response time of 20, 4, and 2.0 min at 25 °C with the S1, S2, and S3 sensing/capture assays, respectively. (B) The pH−response profile of S3 as a function of Hg(II) ion concentrations (0.5 and 1 ppm) obtained at λ_{max} = 496 nm, a response time of 2.0 min, and 25 °C. The inset of B is the effect of pH on Hg(II) ion uptake. (A, B) The profiles indicated the excellent sensing/removal/recovery workability of S1, S2, and S3 at specific pH values of 4.8, 8 and 10.9, respectively.

conditions of the stable donor−acceptor bindings between the **L1**, **L2**, and **L3** receptors and the Hg(II) analyte as well as the formation of [Hg−**L1**], [$(Hg)_2$−**L2**], and [Hg−$(\mathbf{L3})_2$] complexes that colored the membrane sensor disk. The results (Figure 3B and Supporting Information, section S5 and Figure S4) indicate that changes in pH values lead to variations in the colors and reflectance spectra of the Hg(II) ion−MOS (S1, S2, and S3) membrane sensors because of the sensitive changes in the electronic configuration state of the skin-dressing **L1**, **L2**, and **L3** receptors at specific pH values. A notable change in the reflectance intensity of the S1, S2, and S3 membrane sensors at λ_{max} values of 578, 590, and 496 nm was observed at pH 4.8, 8, and 10.9, respectively (Figure 3A,B). The signal response times required for the optimum formation of the color and reflectance spectra of S1, S2, and S3 membrane sensors at pH 4.8, 8, and 10.9 were demonstrated to be 20, 4, and 2 min, respectively, despite the addition of high- or low-dose Hg(II) ion feed solution.

To check the performance of MOS membrane sensors in the sensitive detection/recognition of ultratrace concentrations of Hg(II) ion target, ultraviolet−visible (UV−vis) reflectance spectra were used to quantitatively monitor changes in the optical membrane sensor color upon the addition of Hg(II) ion feed solution to the MOS disks (**S1**, **S2**, and **S3**) fixed into the flow-through module cell detector at the sensing conditions of pH 4.8, 8, and 10.9 and response times of 20, 4, and 2 min, respectively, at 25 °C. The color transition that corresponds to the formation of [Hg−**L1**], [$(Hg)_2$−**L2**], and [Hg−$(\mathbf{L3})_2$] complexes (Scheme 3) provides a simple procedure for the sensitive detection of Hg(II) ions by the naked eye without the use of instruments. The color signaling of MOSs is homogeneous and increases gradually with increasing Hg(II) ion concentration. The concentration-dependent Hg(II) ion quantification was also investigated by simply monitoring UV−vis reflectance spectra under the sensing conditions. The colorimetric determination of Hg(II) ions using MOSs was revealed to be within the detection range from 2.49×10^{-3} to 9.96 μM (Figure 4A−C). The reflectance spectra of the **L1**-, **L2**-, and **L3**-dressed NTs hybrid AAM sensor (S1, S2, and S3) at λ_{max} values of 578, 590, and 496 nm upon adding Hg(II) ions indicate the formation of the charge-transfer [Hg−**L1**], [$(Hg)_2$−**L2**], and [Hg−$(\mathbf{L3})_2$] complexes. The color intensity of the [Hg−**L1**], [$(Hg)_2$−**L2**], and [Hg−$(\mathbf{L3})_2$] complexes increased in linear correlation with Hg(II) ion concentrations up to a maximum visualization plateau, as evident from the standardization curves of Hg(II) ion sensing assays (Figure 4D). The standardization plots of the **L1**-, **L2**-, and **L3**-dressed NTs hybrid AAM sensors generally exhibit a linear correlation (with a standard deviation of 0.6%) at ultratrace concentration levels of Hg(II) ions (Figure 4D and Supporting Information, section 6 and Figure S5). The linear curves indicate that the Hg(II) target concentration is visually detected with human eyes and quantitatively determined with significant sensitivity over a wide range of low concentration levels, even in the presence of actively competitive cations (Figure 4D, dotted lines).[40,41] The LODs of Hg(II) ions for MOSs S1, S2, and S3 are 4.3×10^{-7}, 1.9×10^{-8}, and 3.1×10^{-9} mol/L respectively.[28]

The selective visualization of Hg(II) ions from water sources is important in many areas to avoid the possible adverse health effects of the aforementioned toxicants. A key component of the S1, S2, and S3 membrane sensors technology is its efficiency and selectivity in targeting Hg(II) ions under sensing assay conditions. The influence of the cations and anions that normally interfer with the Hg(II) ion selectivity was investigated for S1, S2, and S3 membrane sensors by initially adding a feed solution of competitive cations and anions with a wide range of tolerance concentrations ranging from 1 to 500 times greater than those of the additive Hg(II) target (T) ions in three controlled sensing assays, namely, single [MOS + ion], binary [MOS + T + ion], and a mixed group of ions [MOS + T + G], under the following target Hg(II) ion sensing conditions: pH values of 4.8, 8, and 10.9 and contact times of 20, 4, and 2 min at 25 °C (Figure 5 and Supporting Information, sections S7 and S8 and Figures S6 and S7).

First, the results show no significant change in the visualization patterns and the spectral signaling responses of the membranes S1, S2, and S3 (blank) at λ_{max} values of 578, 590, and 496 nm, despite the addition of multiple interfering species in a group of ions with high doses of various anions such as F^-, Cl^-, SO_4^{2-}, Br^-, NO_3^{2-}, CO_3^{2-}, IO_3^-, SO_3^{2-}, SCN^-, and PO_4^{3-} and cations such as 10 ppm alkali and alkaline elements [Na(I), Li(I), Sr(II), Cs(I), and Ca(II) ions] or an equivalent dose of actively competitive metal ions of di-,

DOI: 10.1021/acsami.5b02969
ACS Appl. Mater. Interfaces 2015, 7, 13217−13231

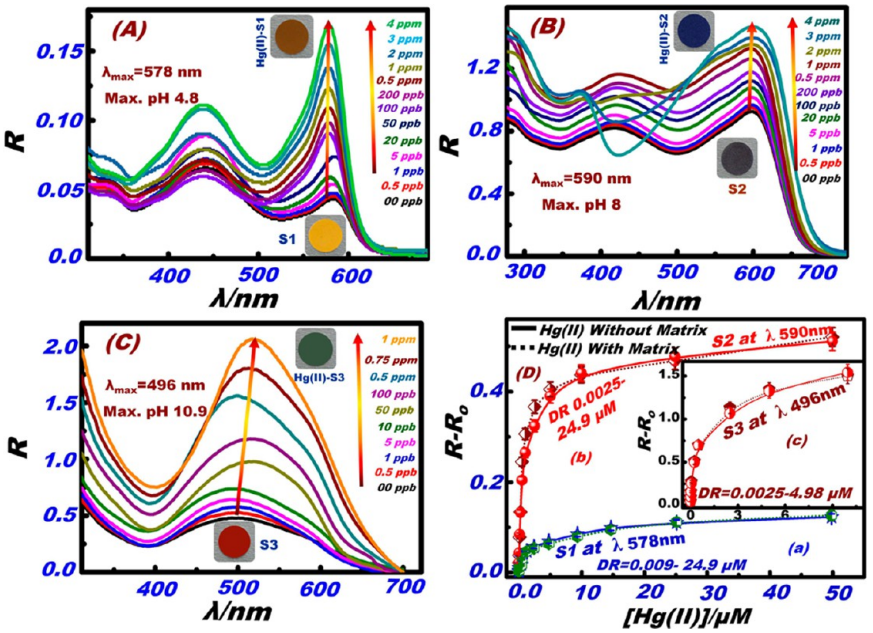

Figure 4. (A–C) Target ion concentration dependence as a function of the reflectance (R) of the MOSs S1, S2, and S3, respectively. The assays (A–C) were obtained with addition of a wide range of Hg(II) ion concentrations from 0 to 5000 μg/L with a response time of 20, 4, and 2 min; volume of 20 mL; and pH value of 4.8, 8, and 10.9, at 25 °C, respectively. Notable changes in color and reflectance intensity of the S1 (A), S2 (B) and S3 (C) at λ_{max} 578, 590, and 496 nm with addition of Hg(II) ion concentrations indicate the simple detection of target ions without needs of sophisticated techniques. (D) Standardization/calibration plots of the reflectance spectra of S1 (a), S2 (b), and S3 (c) for various Hg(II) ion concentrations at λ_{max} 578, 590, and 496 nm; contact time = 20, 4, and 2 min; and temperature = 25 °C, based on the relationship between $R - R_o$ and metal ion concentrations. The inset in the graph shows the detection range (DR) responses of Hg(II) ions. The solid and dotted lines represent the standardization plots of the target ions in the absence and presence of active interfering species [such as Cu(II), Ni(II), Cd(II), Mn(II), Pd(II), Pb(II), Fe(III), Cr(VI), Bi(III), Se(IV), Sb(III), Sn(II), Mo(III), Al(III), Zn(II), and Co(II)] under the same sensing/removal conditions. Note that R and R_o represent the signaling reflectance spectra of the MOSs at λ_{max} 578, 590, and 496 nm, with and without the addition of target Hg(II) ions to S1, S2, and S3 (Da–c), respectively.

tri-, tetra-, and hexavalent elements [Cu(II), Ni(II), Cd(II), Mn(II), Pd(II), Pb(II), Fe(III), Cr(VI), Bi(III), Se(IV), Sb(III), Sn(II), Mo(III), Al(III), Zn(II), and Co(II)] (Figure 5A and Supporting Information). The practical implementation of this ion-selective strategy, including the addition of a group of interfering species to the Hg(II) ion feed solution, revealed that the **L1**-, **L2**-, and **L3**-dressed MOS design is ideal for targeting Hg(II) ion species, with selectivity and specificity at pH 4.8, 8, and 10.9, respectively. Second, in a binary system of a feed solution that contains the Hg(II) target and a competitive cation or anion (Figure 5B,C and Supporting Information, Figures S7 and S8), negative and positive disturbance effects with 1% to 3% change were observed in the reflectance spectra (R) of S1, S2, and S3 membranes (blank) at λ_{max} values of 578, 590, and 496 nm at optimal sensing conditions. Third, to demonstrate the specificity of optical Hg(II) ion–MOS membrane, we examined the reflectance spectra of the **L1**-, **L2**-, and **L3**-dressed MOS design (R_o, blank) upon addition of a single-ion feed solution at λ_{max} values of 578, 590, and 496 nm under optimal sensing conditions. The results show an insignificant change in the reflectance signaling of S1, S2, and S3 with all competitive metal ions (Figure 5B,C), which indicates the weak metal-to-receptor binding events, particularly at pH 4.8, 8, and 10.9. The formation of stable square planar [Hg–**L1**] and [Hg–(**L3**)$_2$] and tetrahedral [(Hg)$_2$–**L2**] complexes, as well as fast Hg-to-receptor binding events, induced a significant change in the reflectance signaling responses at λ_{max} values of 578, 590, and 496 nm, despite the addition of Hg(II) ion to high doses of single, binary, or multiple competitive ion solutions.[45,46]

3.2.2. Potential Durability of Hg(II) ion–MOS sensor. The reusability and durability against repeated use of the MOS membrane sensor/captor represent an essential perspective of green technology, which emphasizes ecological and economic considerations. The concentration ratio of a component between the permeated and input feedwater solution is one of the main determinants of the technical feasibility of a membrane process. Reusability is used to evaluate the MOS sensor design concept of the structural stability of **L1**-, **L2**-, and **L3**-dressed MOS channels and the high performance of the operating MOSs.

This study aims to assess how to efficiently reuse the MOS membrane sensor. With the long-term use of the ion-sensing/filtration setup, the strong binding events of target Hg(II) ions into the **L1**-, **L2**-, and **L3**-dressed mesocage pore in the NT-supported AAM sensor may lead to the following consequences: (1) destruction of the mesoscopic structure and the vertically aligned, rigid NT architectures of the hybrid AAM channels and (2) a decrease in the electron acceptor/donor strength of the **L1**, **L2**, and **L3** receptors, which reduces the optical color signal; thus, Hg(II)-to-receptor binding events modulate weak optical signal response with reuse cycles.

To reuse the MOS membrane sensor/captor, a simple cleanup treatment procedure for the MOS disk was performed. In this process, Hg(II) ions were removed using the benchtop contact technique. First, we vacuum-filtered a monoprotic acid concentration of 0.04 M ClO_4^-, 0.2 M CH_3COO^-, and 0.5 M ClO_4^- to extract or elute Hg(II) ions from the pore openings of the Hg(II)–**S1**, Hg(II)–**S2**, and Hg(II)–**S3** surfaces and pores (Schemes 1 and 2). The actively acidic H^+ character of $HClO_4$

DOI: 10.1021/acsami.5b02969
ACS Appl. Mater. Interfaces 2015, 7, 13217–13231

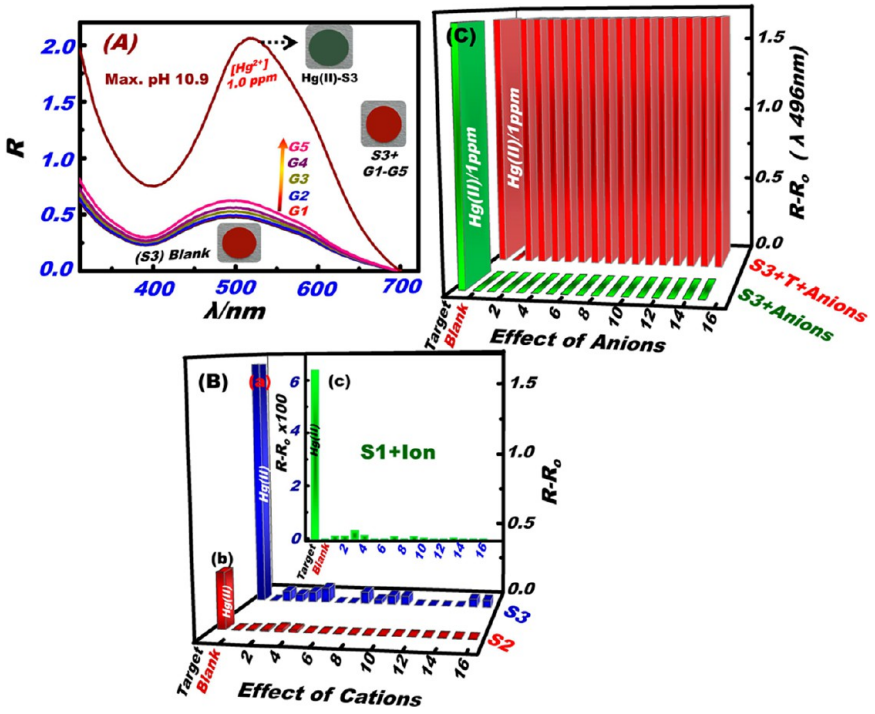

Figure 5. Studies of the selective sensing and removal for the Hg(II) ion−MOSs upon addition of interfering species in three different assay systems: single (i.e., MOS + ion), binary (i.e., MOS + T + ion), and a group of interfering ions (i.e., MOS + T + G). (A) Effect of addition of a feed solution containing a group of interfering cations (i.e., G1−G5) with tolerance concentrations 1−50 times greater than those of the additive (1 ppm) Hg(II) target ions on the color response and signaling reflectance spectra of S3 at λ_{max} 496 nm and pH 10.9, where G1 contains Na^+, Li^+, K^+, and Ca^{2+}; G2 contains Sr^{2+}, Cr^{6+}, Al^{3+}, and Mg^{2+}, and Ni^{2+}; G3 contains Mo^{3+}, Sn^{2+}, Sb^{3+}, and Mn^{2+}; G4 contains Zn^{2+}, Pd^{2+}, Cd^{2+}, and Bi^{3+}; and G5 contains Fe^{3+}, Se^{4+}, Co^{2+}, and Cu^{2+}. (B) Study of the effect of the addition of each interfering ion (single system) on MOSs S1, S2, and S3 at λ_{max} 578, 590, and 496 nm and pH 4.8, 8, and 10.9, respectively. (C) Study of the effect of the added anions in both single and binary sensing/removal assays for S3 at λ_{max} 496 nm and pH 10.9. For part B, the interfering cations are listed in the order (1) Co(II), (2) Cu(II), (3) Ni(II), (4) Fe(III), (5) Na(I), (6) Ca(II), (7) Mn(II), (8) Pd(II), (9) Pb(II), (10) Bi(III), (11) Cd(II), (12) Cr(IV), (13) Li(I), (14) Cs(I), (15) Sr(II), and (16) Se(IV). For part C, the interfering anions are listed in the order (1) NO_3^-, (2) F^-, (3) Cl^-, (4) SO_4^{2-}, (5) Br^-, (6) NO_3^{2-}, (7) CO_3^{2-}, (8) IO_3^-, (9) SO_3^{2-}, (10) PO_4^{3-}, (11) tartrate, (12) citrate, (13) oxalate, (14) malonate, (15) carbonate, and (16) silicate and acetate.

and CH_3COOH stripping agents has the ability to destabilize the Hg^{2+}-to-L binding events of the [Hg−**L1**], [$(Hg)_2$−**L2**], and [Hg−$(\mathbf{L3})_2$] complexes during the stripping process.[54] In this Hg^{2+} ion recovery (collection) mechanism, the ClO_4^- agent, for example, displaces the ligand from the Hg(II)-to-L chelation through the formation of an intermolecular $ClO_4^-\cdots Hg^{2+}\cdots$L chelate, subsequently extracting the Hg(II) ion from Hg(II)−L immobilized on MOSs surfaces. In order to driven this time-dependent decomplexation process, the stability constant (log K_s) of the developed [Hg−$(CH_3COO)_2$] and [Hg−$(ClO_4)_2$] complexes are approximately 8.3 and 25.4, respectively, which are higher than that of Hg(II)−L at the MOSs surfaces, consistent with the calculated log K_2 of these [Hg−$(CH_3COO)_2$] and [Hg−$(ClO_4)_2$] complexes in solution.[54,55] The complete collection of Hg(II) ions from the MOS membrane channels was investigated by analyzing the filtrate solution and the solid MOS membrane disk using ICP−MS and UV−vis spectroscopy (Figure 6), respectively. The result shows the reusability of the MOS membrane sensor/captor during Hg(II) ion extraction cycles. MOS membrane sensors/captors retained approximately 90% of their main efficiency after six washing/reuse cycles (Figure 6B). This experimental finding indicates the following three major components: (1) The toxicity control, monitoring, and selective collection of trapped Hg(II)species via a chemical stripping agent (Scheme 3), which leads to a reduction in the adverse health risks of releasing this Hg(II) toxicant; (2) the feasibility of the solid MOS membrane sensor/captor, in which the MOSs can be repeatedly recycled with no negative changes in the unique mesosponge cagelike sink architectures or fouling the membrane via the precipitation of metal salts with the reuse cycle; and (3) the simple releasing process of the Hg(II) target from the sensor disk concentrates. The volume-enabled controlled waste management of the collected elements has an efficiency of 99% (Scheme 1).

The constructed sensing designs, combined with the simple reusability process, may open the door to integrating and validating technological solutions into the overall water cycle, including the production of drinking and processed water as well as industrial wastewater and groundwater treatment.

3.2.3. Hg(II) Ion Removal Functionality of Membrane. By following the membrane sensing functionality based visual detection, recognition, and selective monitoring, our designed membrane sensor/captor systems can be employed to deliver ultrapure water by selectively removing and capturing trace levels of Hg(II) ion contaminants. To check the selective removal of Hg(II) ions, benchtop adsorption assays were conducted by adding a wide range of Hg^{2+} ion concentrations in the absence of actively interfering components to fixed one-layer disks of MOS (S1, S2, and S3) membrane sensors/captors (see Supporting Information, sections S9 and S10 and Figures S8 and S9).[56,57] To study the selective Hg(II) ion removal, we added a feed solution containing an equivalent dose of the actively interfering group of cations [Na(I), Ca(II), Cd(II),

DOI: 10.1021/acsami.5b02969
ACS Appl. Mater. Interfaces 2015, 7, 13217−13231

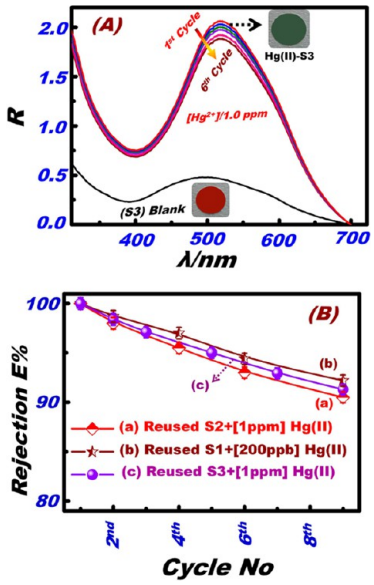

Figure 6. (A) Reusability studies of S3 in terms of the spectral reading changes (R) for the detection and removal of 1 ppm of Hg(II) after six regeneration/reuse cycles at pH 10.9. (B) The Hg(II) ion rejection efficiency (E%) of the MOSs S1 (b), S2 (a), and S3 (c) at pH 4.8, 8, and 10.9; feed solution volume of 20 mL; and contact time of 20, 4, and 2 min, at 25 °C. The E% was calculated from the %($C_o - C_p/C_o$) ratio of Hg(II) ion concentration of outlet filtrate/permeate (C_p/μM) per cycle and the initial feed concentration (C_o/μM). Note: the E% calculation was determined by ICP−MS analysis; however, the reflectance spectra indicating the visual change of the MOSs membranes after adsorption of Hg(II) ions were monitored by UV−visible spectroscopy.

Mn(II), Pd(II), Pb(II), Fe(II), Cr(VI), and Bi(III)] and Hg(II) ion to MOS S3 membrane at pH 10.9, pressure 50 kPa, and 25 °C, in a total volume of 20 mL (Supporting Information, Figure S9). We applied the Langmuir and Freundlich isotherms at equilibrium as theoretical models for monolayer adsorption.[46] Our results reveal an increase in the adsorption amount (q_e, mg g^{-1}) of membrane sensor/captor with increasing Hg(II) ion concentration at equilibrium, which indicates the applicability of removing a wide range of Hg(II) ion concentrations without preconcentration in both assays (i.e., presence and absence of interference). The maximum uptake value (q_e) of Hg(II) ions are 71, 175, and 299 mg/g for S1, S2, and S3, respectively, at 25 °C (see Supporting Information, sections S9 and S10). The straight line of the C_e/q_e versus C_e plot (Supporting Information, Figures S8 and S9) of both adsorption assays confirms the formation of the monolayer metal coverage on the AAM channels of the S1 and S3 membranes incorporated with interior mesocage NTs. However, the linear plot of log q_e versus log C_e shows that the adsorption of Hg(II) on S2 and S3 follows the Freundlich isotherm (Supporting Information, Figures S8 and S9). For example, Figure S8 (Supporting Information) shows the adsorption capacity (q_m) of Hg(II) ions from the buffer medium (at pH 10.9) with high efficiencies for both adsorption assays [0.271 and 0.262 g of Hg(II) ion/g of MOS (S3) captor, respectively]. The slight decrease in the practical q_m (~5%) of the Hg(II) adsorption assay among a group of interfering ions indicates Hg(II) ion selective removal using MOS under batch-contact adsorption conditions.

To investigate the reversibility feature of the adsorption/desorption assays, kinetic studies were conducted on batch-contact Hg(II) ion adsorption/desorption assays at 25 °C. However, the desorption process was conducted by adding a stripping agent that effectively removes trapped Hg(II) ions from the mesocage pores in NTs dressed with **L1**, **L2**, and **L3** chelating agents. The experimental finding shows a time-dependent Hg(II) ion release into the surrounding solution, as evident from ICP−MS analyses of backside filtrates. For example, trapped Hg(II) ions in **S3** will desorb slowly when exposed to a 0.5 M concentration of the ClO_4^- agent, as indicated by the considerable adsorption/desorption rate ratios (k_1/k_{-1}) of 3.995 and 2.021 for Hg(II) ion removal assays in both the absence and presence of interference, respectively. This finding indicates that the Langmuir equilibrium constant K_L values are consistent with the ratio of adsorption/desorption rates of Hg(II) ion (k_1/k_{-1}), which shows that Hg(II) adsorption assays are fully reversible. Furthermore, a large K_L value indicates two key features of the MOS membrane sensor/captor system: (1) the desorption process has occurred mainly from the interior cavities of NTs hybrid MOS membrane channels and (2) the Hg(II)-to-receptor binding events are strong.

To illustrate the effectiveness of using MOS membranes for water purification to remove Hg(II) ion toxicant, we have statistically valued the adsorption performance in terms of the maximum adsorption capacity (q_m, mg g^{-1}) of the Hg(II) ions using a hierarchical membrane sensor/captor instead of commercial and established membrane scaffolds (Figure 7).

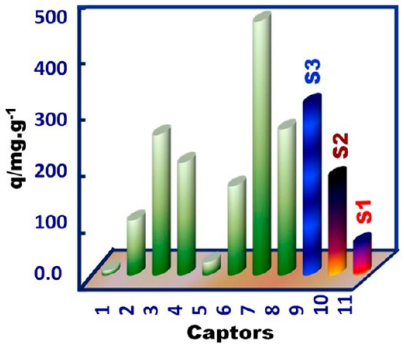

Figure 7. Representative distribution diagram for adsorption capacities (q, mg g^{-1}) of Hg(II) ions onto various functionalized material "adsorbents" collected from the literature in comparison with the fabricated MOS membranes. Note, the specification and components of captors (i.e., 1−11) are listed in Table 1

Our findings indicate that although our membrane sensor/captor shows a mediated q_m value, it may function as an effective and selective adsorbent of ultratrace Hg(II) ion concentration for all membranes used, such as modified silica, alumina, activated carbon, and synthetic polymers[58−65] (Table 1 and Figure 7). Moreover, apart from colorimetric detection, recognition, and removal functionalities in one-step screening, the substantial adsorption efficiency of MOS membrane captors is receiving significant interest as a potentially effective solution to a growing range of water purification and separation needs.[66−68]

3.2.4. Membrane Rejection/Filtration Workability. As a part of the adequate supply of water with suitable qualities to meet human, environmental, and industrial needs, we focus on the selective membrane separation/filtration of an individual toxic cation (i.e., Hg^{2+} ion) among heterogeneous and competitive matrices. Regarding the filtration system, two

DOI: 10.1021/acsami.5b02969
ACS Appl. Mater. Interfaces 2015, 7, 13217−13231

Table 1. Comparison of the Adsorption Capacities of Hg(II) Ion Captors/Adsorbents Functionalized with a Variety of Chelating Agents onto Solid Scaffold Materials

captor	incorporated ligand	solid support	adsorption capacity (q)/mg g^{-1}	refs
1	tetraphenylporphine tetrasulfonic acid (TPPS)	silica	9.1	58
2	humic acid	alumina	97.70	59
3	tetrakis(3-hydroxyphenyl)porphyrin	methacrylic acid-ethylene glycol dimethacrylate polymer	249.00	60
4	trioctylmethylammonium chloride	activated carbon	200.00	61
5	amino group	magnetic graphene	23.03	62
6		$CoFe_2O_4$-reduced graphene oxide	157.90	63
7	2-amino-5-mercapto-1,3,4-thiadiazole	mesoporous carbon (CMK-3)	450.45	64
8	lysine Schiff-base	cellulose	258.75	65
9	L1-dressed membrane	S1	57.4	this work
10	L2-dressed membrane	S2	175	this work
11	L3-dressed membrane	S3	271	this work

important key components must be considered, namely, the hierarchal structure stability of the membrane platform and the Hg(II) ion selectivity procedure (Scheme 2). Both key components led the design of **L1**-, **L2**-, and **L3**-dressed MOSs that will be used as a model system for the following phenomena: (1) the selective capture and binding (rejection) of Hg(II) ion toxicants even at trace concentrations and among the most competitive cations in the MOS cavity-supported NTs and (2) the transport of desired ions (i.e., nontoxicants) along the gradient across the designed membrane sensor channels (permeation) that was driven by pressure-assisted solute diffusion. Using a benchtop contact technique, the rejection/permeation process that is responsible for the specificity of ion transport across MOS membrane channels significantly depends on the pH value of the feed solution of Hg(II) ions under rejection/permeation conditions at a pressure-assisted force of 50 kPa and contact times of 20, 4, and 2 min at 25 °C (Figure 8). This finding indicates that the maximum rejected

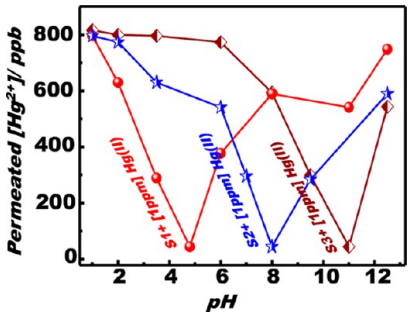

Figure 8. Study of the effect of pH values on the filtration/separation assays of the MOS (S1, S2, and S3) membranes with 1 ppm of Hg^{2+} ion feed solution at pressure 50 kPa, volume 20 mL, and 25 °C. The feed (C_o) and outlet filtrate (permeated) (C_p) solutions were quantitatively analyzed using ICP−MS analysis.

Hg(II) ion concentration in S1, S2, and S3 was found at pH 4.8, 8, and 10.9, respectively, as evidenced from the reflectance signaling responses of the solid Hg(II)−MOS disks (Figure 8).

We also study the rejected/permeated Hg(II) ion concentration of MOS S3 membrane as a function of contact time by monitoring the permeate (C_p) and rejected ($C_o - C_p$) solution of Hg(II) ions using ICP−MS analyses at pH 10.9 with a volume of 20 mL at 25 °C (Figure 9). The selective removal of Hg(II) ions (rejected) into mesocage NTs/AAM sensor channels was confirmed visually and quantitatively by recording the reflectance spectra of MOS S3 membrane disk at a λ_{max}

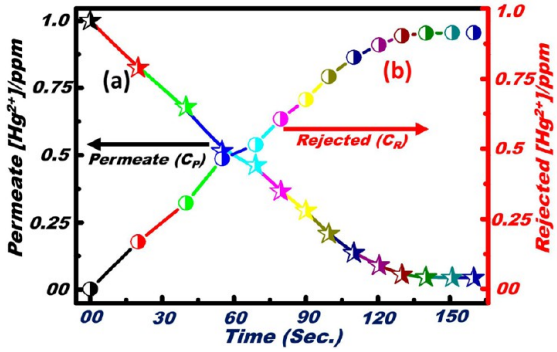

Figure 9. Time-dependent filtration assay of permeated (C_p)/rejected (C_R) Hg(II) ion concentration using MOS S3 with addition of 1 ppm of Hg(II) ion in feed solution (a and b, respectively). The feed (C_o) and outlet filtrate (permeated) (C_p) solutions were quantitatively analyzed using ICP−MS analysis. The concentration of Hg(II) ion rejected solution (C_R) was determined as follows: $C_R = C_o - C_p$. The rejection/filtration assays were conducted by using double disks of S3 membrane and addition of feed solution at pH 10.9, pressure 50 kPa, and a total volume of 20 mL, at 25 °C.

value of 496 nm as a result of the formation of strong Hg(II)−**L3** binding events at varying times. Figure 9 shows that the rejected Hg(II) ion concentration (C_R) was significantly increased with increasing contact time, whereas that of the permeate solution (C_p) was decreased. The rejected and inverse permeated curves of the Hg(II) ion concentration assay (Figure 9) may reach their saturation state within 2 min. Both curves indicate the practical removal of >96% Hg(II) ions in the MOS membrane sensor/captor channels. Within a contact time of ≥2 min, two important key values should be considered in water purification and separation needs using S3 membrane: (1) the filtrate solution contains water free of Hg(II) ion toxicant (Scheme 1) and (2) the MOS membranes enable multiscale system optimization with respect to their sensing/capture/filtration functionalities, which leads to controlled visual detection, quantitative recognition, and selective removal of Hg(II) ions in a one-step screening assay.

3.2.5. Real Hg(II) Ion Recovery from Water Sources in Saudi Arabia. To validate the practicality of the designed MOS membranes in the selective recovery process of Hg(II) ions from actual contaminated samples, two pretreated real sample effluents were collected from tap and underground water sources in Abha City, Saudi Arabia, and used as precursor sources to test the practical implementation of the MOS membrane sensors/captors in Hg(II) ion recovery (Table 2 and

DOI: 10.1021/acsami.5b02969
ACS Appl. Mater. Interfaces 2015, 7, 13217−13231

Table 2. Applicability of the MOS S3 Membrane toward Hg(II) Ion Recovery of Hg(II) from Tap, Underground, and Simulated Water Samples Containing Multimixture Matrices under the Benchtop Contact Conditions Using Double-Layer Disks of S3, 40 mL Feed Solution Volume at pH 10, Contact Time ≥10 min, and 25 °C[a]

water sample	concn of foreign ions/ppm	C_o/ppm	C_R/ppm	C_p/ppm	C_c/ppm	% recovery
real tap	Na(I), 35.2; K(I), 9.055; Li(I), 0.03; Mg(II), 4.4; Ca(II), 15.5; Co(III), 0.002; V(II), 0.009; Zn(II), 0.005; Mn(II), 0.011; Cr(VI), 0.002; Sr(II), 0.05; Fe(III), 0.015; Al(III), 0.007	0.028 ± 0.004	0.0255 ± 0.005	0.0025 ± 0.0006	0.0245 ± 0.005	87.5
underground	Na(I), 62.2; K(I), 8.6; Li(I), 0.015; Mg(II), 10.4; Ca(II), 33.5; Co(III), 0.002; V(II), 0.019; Be(II), 0.02; Zn(II), 0.009; Mn(II), 0.016; Cr(VI), 0.004; Sr(II), 0.29; Fe(III), 0.02; Al(III), 0.012	0.082 ± 0.005	0.079 ± 0.004	0.003 ± 0.0005	0.0774 ± 0.004	94.3
simulated ref	Na(I), 60; K(I), 10; Li, 0.02; Mg(II), 10; Ca(II), 35; Co(III), 0.005; V(II), 0.02; Be(II), 0.02; Zn(II), 0.01; Mn(II), 0.02; Cr(VI), 0.005; Sr(II), 0.3; Fe(III); 0.03; Al(III), 0.02	0.050 ± 0.008	0.04873 ± 0.006	0.0127 ± 0.004	0.0479 ± 0.007	95.8

[a]The initial (C_o), rejected (C_R), permeated (C_p), and recovery (C_c) concentrations of Hg(II) ions was determined by ICP−MS. The % recovery = C_c/C_o ratio, where C_c is the Hg(II) target ion concentration released in solution by stripping agent.

Figure 10). The initial samples of tap and underground water were found to contain 0.028 and 0.082 ppm of Hg(II) analytes,

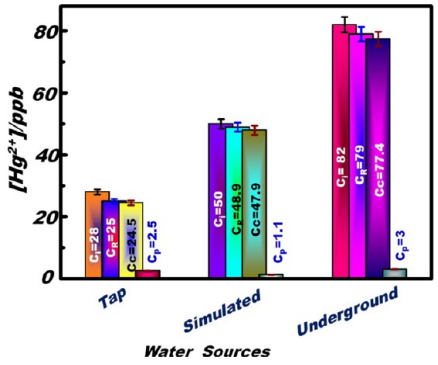

Figure 10. Real applicability of the MOS S3 membrane toward the effective recovery of Hg(II) ion analyte from the tap and underground water samples containing multimixture matrices under the benchtop contact conditions using double-layer disks of optical membrane sensor/captor, 40 mL feed solution volume at pH 10.9, contact time ≥10 min, and at 25 °C. The simulated sample (i.e., reference) was also studied under the same ion-recovery conditions. The initial (C_o), rejected (C_R), permeated (C_p), and recovery (C_c) concentrations of Hg(II) ions were determined by ICP−MS.

respectively, and other metal matrices at different concentration levels ranging from 0.002 to 62.2 ppm, such as Na(I), K(I), Li(I), Mg(II), Ca(II), Co(III), V(II), Be(II), Zn(II), Mn(II), Cr(VI), Sr(II), Fe(III), and Al(III) ions, as analyzed via ICP−MS, consistent with previously provided analyses in other works.[69] We used the benchtop contact technique with a double-layer disks of MOS S3 membrane to selectively recover Hg(II) ions from a sample with 40 mL volume, pH 10.9, and a contact time of ≥10 min at 25 °C.

The rejected and permeated Hg(II) ion analytes from the tap and underground water samples that contain multimixture matrices are summarized in Table 2 and Figure 10. The analytical data show that >91% of Hg(II) ions was extracted using one-step removal screening. The filtered tap and underground water solutions (permeate) that contain 2.5 and 3.0 μg/L toxic Hg(II) ion concentrations, respectively, are barely similar to the permissible levels of toxic Hg(II) ions in drinking water (i.e., 2 μg/L).[19,70] The decrease in rejected or permeated Hg(II) ions from the actual tap or underground water samples compared with those removed (≥97%) from the simulated sample (i.e., reference) provides high-quality (filtrated) water with Hg(II) ion concentration levels that are far below the permissible level (Table 2). This finding indicates the minimal effects of ion-system compositions (i.e., interferences from the major matrix elements and biological species) on the final recovery of Hg(II). The last stage involves recovery experiments using a stripping agent of 0.5 M ClO_4^- (Schemes 1 and 3) to release Hg(II) ions from MOS S3 and obtain ion-free MOS S3 surfaces. Using the benchtop contact technique with fixed Hg(II)−S3 membrane disks, we vacuum filtered the 0.5 M ClO_4^- stripping agent to effectively remove the trapped Hg(II) ions in MOS S3 pore surfaces. After five or more washing/reusing cycles, the collected Hg(II) ion solution (C_c) was analyzed via ICP−MS. The results indicate that ≥98% of Hg(II) ions was released by this simple chemical treatment (Table 2). These analytical data indicate that the proposed method using MOS membranes can be a potential candidate for actual environmental remediation and pollution control of water sources.

4. CONCLUSION

MOSs were fabricated through skin-dressed layers of organic active **L1**, **L2**, and **L3** colorants by following the vertical alignment and open surfaces of the top−bottom ends of NTs in AAM channels. The synthetic protocol provided long-term retention of **L1**, **L2**, and **L3** receptors in uniform alignment that filled in the interconnected, tubular, and 3D nanosized cagelike pores in uniformly shaped NTs hybrid AAM scaffolds. The pH-dependent Hg(II) ion sensing system showed three key features, namely, (1) visual detection, (2) sensitivity, and (3) selectivity. The practical implementation of the simple membrane sensor is its selectivity. However, the **L1**-, **L2**-, and **L3**-dressed MOSs are ideal for targeting Hg(II) ion species in heterogeneous mixtures with inorganic cations and anions as well as organic bulk molecules. Our results show the feasibility of the solid MOS membrane, in which MOS membrane disks can be repeatedly recycled without damaging the hierarchical mesosponge sinks or fouling the membrane via the precipitation of metal salts in the reuse cycle. The simple releasing process of the Hg(II) target from the MOS disk involves concentrating the collected elements, reducing their volume, and enabling controlled waste management at ≥97% efficiency. Apart from its colorimetric detection, recognition, and removal functionalities in a one-step screening system, the substantial adsorption efficiency of the MOS membrane sensors/captors is arousing significant interest as a potential and effective solution to the widening range of water

DOI: 10.1021/acsami.5b02969
ACS Appl. Mater. Interfaces 2015, 7, 13217−13231

purification and separation needs. The MOS membrane filtration protocol based Hg(II) ion rejection and permeation of nonselective elements may lead to two key values that must be considered in water purification and separation needs: (1) the filtrate solution contains water free of Hg(II) ion toxicant and (2) the sensor/captor array enables multiscale system optimizations with respect to sensing/capture/filtration processing functionalities. Notably, the practical feasibility of the designed MOS membrane sensor/captor arrays toward the selective recovery process of Hg(II) ions from actual contaminated samples collected from tap and underground water sources in Abha City, Saudi Arabia, was achieved. The real analytical data of the proposed method indicate that MOSs can serve as a potential candidate for hazard remediation and control in water sources.

■ ASSOCIATED CONTENT

Supporting Information

Details of the material characterization, ^{29}Si MAS NMR analysis, method for fabricating MOS membrane, solubility of inorganic divalent mercury species, pH-dependent response profiles, linear range in standardization curves, selectivity studies of the Hg(II) ion−MOSs, Langmuir and Freundlich isotherms for the adsorption of Hg(II) ions, and selective removal/adsorption isotherms of Hg(II) ions are presented. The Supporting Information is available free of charge on the ACS Publications website at DOI: 10.1021/acsami.5b02969.

■ AUTHOR INFORMATION

Corresponding Author

*Tel: +81-298592135. Fax: +81-298592025. E-mail: sherif.elsafty@nims.go.jp; sherif@aoni.waseda.jp.

Notes

The authors declare no competing financial interest.

■ ACKNOWLEDGMENTS

This work was supported by the Prince Sattam Bin Abdulaziz University (Saudi Arabia). The authors would like to thank Dr. Abdulrahman Al-Assemi (Rector of Prince Sattam Bin Abdulaziz University) and Dr. Rashed Al-Rushood (Dean of Al-Aflaj College of Science and Human Studies) for their supporting and encouragement during this work.

■ REFERENCES

(1) Martin, C. R. Membrane-Based Synthesis of Nanomaterials. *Chem. Mater.* **1996**, *8*, 1739−1746.
(2) Meoto, S.; Coppens, M. Anodic Alumina-Templated Synthesis of Mesostructured Silica Membranes—Current Status and Challenges. *J. Mater. Chem. A* **2014**, *2*, 5640−5654.
(3) Kickelbick, G. Formation of Hexagonal Mesoporous Silica in Submicrometer Channels. *Small* **2005**, *1*, 168−170.
(4) Wu, Y.; Livneh, T.; Zhang, Y. X.; Cheng, G.; Wang, J.; Tang, J.; Moskovits, M.; Stucky, G. D. Templated Synthesis of Highly Ordered Mesostructured Nanowires and Nanowire Arrays. *Nano Lett.* **2004**, *4*, 2337−2342.
(5) El-Safty, S. A.; Shahat, A.; Warkocki, W.; Ohnuma, M. Building-Block-Based Mosaic Cage Silica Nanotubes for Molecular Transport and Separation. *Small* **2011**, *7*, 62−65.
(6) Han, W. S.; Lee, H. Y.; Jung, S. H.; Lee, S. J.; Jung, J. H. Silica-Based Chromogenic and Fluorogenic Hybrid Chemosensor Materials. *Chem. Soc. Rev.* **2009**, *38*, 1904−1915.
(7) Kim, H. N.; Lee, M. H.; Kim, H. J.; Kim, J. S.; Yoon, J. A New Trend in Rhodamine-Based Chemosensors: Application of Spirolactam Ring-Opening to Sensing Ions. *Chem. Soc. Rev.* **2008**, *37*, 1465−1472.
(8) Lee, S. J.; Lee, J.-E.; Seo, J.; Jeong, I. Y.; Lee, S. S.; Jung, J. H. Optical Sensor Based on Nanomaterial for the Selective Detection of Toxic Metal Ions. *Adv. Funct. Mater.* **2007**, *17*, 3441−3446.
(9) Jin, K.; Yao, B.; Wang, N. Structural Characterization of Mesoporous Silica Nanowire Arrays Grown in Porous Alumina Templates. *Chem. Phys. Lett.* **2005**, *409*, 172−176.
(10) Lee, K. J.; Min, S. H.; Jang, J. Vapor-Phase Synthesis of Mesostructured Silica Nanofibers inside Porous Alumina Membranes. *Small* **2008**, *4*, 1945−1949.
(11) Gong, Z.; Ji, G.; Zheng, M.; Chang, X.; Dai, W.; Pan, L.; Shi, Y.; Zheng, Y. Structural Characterization of Mesoporous Silica Nanofibers Synthesized within Porous Alumina Membranes. *Nanoscale Res. Lett.* **2009**, *4*, 1257−1262.
(12) Yang, Z.; Niu, Z.; Cao, X.; Yang, Z.; Lu, Y.; Hu, Z.; Han, C. C. Template Synthesis of Uniform 1d Mesostructured Silica Materials and Their Arrays in Anodic Alumina Membranes. *Angew. Chem., Int. Ed.* **2003**, *42*, 4201−4203.
(13) Hill, J. J.; Cotton, S. P.; Ziegler, K. J. Alignment and Morphology Control of Ordered Mesoporous Silicas in Anodic Aluminum Oxide Channels by Electrophoretic Deposition. *Chem. Mater.* **2009**, *21*, 1841−1846.
(14) Yoo, S.; Ford, D. M.; Shantz, D. F. Synthesis and Characterization of Uniform Alumina−Mesoporous Silica Hybrid Membranes. *Langmuir* **2006**, *22*, 1839−1845.
(15) Martin, C. R.; Siwy, Z. Molecular Filters: Pores within Pores. *Nat. Mater.* **2004**, *3*, 284−285.
(16) El-Safty, S. A. Designs for Size-Exclusion Separation of Macromolecules by Densely-Engineered Mesofilters. *TrAC Trends Anal. Chem.* **2011**, *30*, 447−458.
(17) Clarkson, T. W.; Magos, L.; Myers, G. J. The Toxicology of Mercury—Current Exposures and Clinical Manifestations. *N. Engl. J. Med.* **2003**, *349*, 1731−1737.
(18) Cerulli, N.; Campanella, L.; Grossi, R.; Politi, L.; Scandurra, R.; Soda, G.; Gallo, F.; Damiani, S.; Alimonti, A.; Petrucci, F.; Caroli, S. Determination of Cd, Cu, Pb and Zn in Neoplastic Kidneys and in Renal Tissue of Fetuses, Newborns and Corpses. *J. Trace Elem. Med. Biol.* **2006**, *20*, 171−179.
(19) El-Safty, S. A.; Shenashen, M. A.; El-Safty, S. A. Mercury-Ion Optical Sensors. *TrAC Trends Anal. Chem.* **2012**, *38*, 98−115.
(20) Oken, E.; Wright, R. O.; Kleinman, K. P.; Bellinger, D.; Amarasiriwardena, C. J.; Hu, H.; Rich-Edwards, J.; Gillman, M. W. Maternal Fish Consumption, Hair Mercury, and Infant Cognition in a U.S. Cohort. *Environ. Health Perspect.* **2005**, *113*, 1376−1380.
(21) Harris, H. H.; Pickering, I. J.; George, G. N. The Chemical Form of Mercury in Fish. *Science* **2003**, *301*, 1203−1203.
(22) Coronado, E.; Galán-Mascarós, J. R.; Martí-Gastaldo, C.; Palomares, E.; Durrant, J. R.; Vilar, R.; Gratzel, M.; Nazeeruddin, M. K. Reversible Colorimetric Probes for Mercury Sensing. *J. Am. Chem. Soc.* **2005**, *127*, 12351−12356.
(23) Chen, Y.; Tong, J.; D'Ulivo, A.; Belzile, N. Determination of Mercury by Continuous Flow Cold Vapor Atomic Fluorescence Spectrometry Using Micromolar Concentration of Sodium Tetrahydroborate as Reductant Solution. *Analyst* **2002**, *127*, 1541−1546.
(24) Anthemidis, A. N.; Zachariadis, G. A.; Michos, C. E.; Stratis, J. A. Time-Based Injection On-Line Preconcentration Cold Vapour Generation Procedure for Ultra-Trace Mercury Determination with Inductively Coupled Plasma Atomic Emission Spectrometry. *Anal. Bioanal. Chem.* **2004**, *379*, 764−769.
(25) Vallant, B.; Kadnar, R.; Goessler, W. Development of A New HPLC Method for the Determination of Inorganic and Methylmercury in Biological Samples with ICP−MS Detection. *J. Anal. At. Spectrom.* **2007**, *22*, 322−325.
(26) Ros-Lis, J. V.; Marcos, M. D.; Mártinez-Máñez, R.; Rurack, K.; Soto, J. A Regenerative Chemodosimeter Based on Metal-Induced Dye Formation for the Highly Selective and Sensitive Optical Determination of Hg^{2+} Ions. *Angew. Chem., Int. Ed.* **2005**, *44*, 4405−4407.

DOI: 10.1021/acsami.5b02969
ACS Appl. Mater. Interfaces 2015, 7, 13217−13231

(27) Kim, S. H.; Kim, J. S.; Park, S. M.; Chang, S. Hg^{2+}-Selective Off−On and Cu^{2+}-Selective On−Off Type Fluoroionophore Based Upon Cyclam. *Org. Lett.* **2006**, *8*, 371−374.
(28) Lee, M. H.; Lee, S. W.; Kim, S. H.; Kang, C.; Kim, J. S. Nanomolar Hg(II) Detection Using Nile Blue Chemodosimeter in Biological Media. *Org. Lett.* **2009**, *11* (10), 2101−2104.
(29) Zhao, Y.; Lin, Z.; He, C.; Wu, H.; Duan, C. A. Turn-On Fluorescent Sensor for Selective Hg(II) Detection in Aqueous Media Based on Metal-Induced Dye Formation. *Inorg. Chem.* **2006**, *45*, 10013−10015.
(30) Liu, J.; Lu, Y. Stimuli-Responsive Disassembly of Nanoparticle Aggregates for Light-Up Colorimetric Sensing. *J. Am. Chem. Soc.* **2005**, *127*, 12677−12683.
(31) Yang, X.; Li, Y.; Bai, Q. A Highly Selective and Sensitive Fluorescein-Based Chemodosimeter for Hg^{2+} Ions in Aqueous Media. *Anal. Chim. Acta* **2007**, *584*, 95−100.
(32) Mello, J. V.; Finney, N. S. Reversing the Discovery Paradigram: A New Approach to the Combinatorial Discovery of Fluorescent Chemosensors. *J. Am. Chem. Soc.* **2005**, *127*, 10124−10125.
(33) Guo, X.; Qian, X.; Jia, L. A Highly Selective and Sensitive Fluorescent Chemosensor for Hg^{2+} in Neutral Buffer Aqueous Solution. *J. Am. Chem. Soc.* **2004**, *126*, 2272−2273.
(34) Moon, S.; Youn, N. J.; Park, S. M.; Chang, S. Diametrically Disubstituted Cyclam Derivative Having Hg^{2+}-Selective Fluoroionophoric Behaviors. *J. Org. Chem.* **2005**, *70*, 2394−2397.
(35) Ono, A.; Togashi, H. Highly Selective Oligonucleotide-Based Sensor for Mercury(II) in Aqueous Solutions. *Angew. Chem., Int. Ed.* **2004**, *43*, 4300−4302.
(36) Lakshmi, D.; Sharma, P. S.; Prasad, B. B. Imprinted Polymer-Modified Hanging Mercury Drop Electrode for Differential Pulse Cathodic Stripping Voltammetric Analysis of Creatine. *Biosens. Bioelectron.* **2007**, *22*, 3302−3308.
(37) Maghasi, A. T.; Conklin, S. D.; Shtoyko, T.; Piruska, A.; Richardson, J. N.; Seliskar, C. J.; Heineman, W. R. Spectroelectrochemical Sensing Based on Attenuated Total Internal Reflectance Stripping Voltammetry. 2. Determination of Mercury and Lead. *Anal. Chem.* **2004**, *76*, 1458−1465.
(38) El-Safty, S. A.; Shenashen, M. A.; Shahat, A. Tailor-Made Micro-Object Optical Sensor Based on Mesoporous Pellets for Visual Monitoring and Removal of Toxic Metal Ions from Aqueous Media. *Small* **2013**, *9*, 2288−2296.
(39) Nazeeruddin, M. K.; Censo, D. D.; Humphry-Baker, R.; Gratzel, M. Highly Selective and Reversible Optical, Colorimetric, and Electrochemical Detection of Mercury(II) by Amphiphilic Ruthenium Complexes Anchored onto Mesoporous Oxide Films. *Adv. Funct. Mater.* **2006**, *16*, 189−194.
(40) El-Safty, S. A.; Abdellatef, S.; Ismael, M.; Shahat, A. Optical Nanosphere Sensor Based on Shell-by-Shell Fabrication for Removal of Toxic Metals from Human Blood. *Adv. Healthcare Mater.* **2013**, *2*, 854−862.
(41) Shenashen, M. A.; El-Safty, S. A.; Elshehy, E. A. Architecture of Optical Sensor for Recognition of Multiple Toxic Metal Ions from Water. *J. Hazard. Mater.* **2013**, *260*, 833−843.
(42) Jacobi, Z. E.; Li, L.; Liu, J. Visual Detection of Lead(II) Using a Label-Free DNA-Based Sensor and Its Immobilization within a Monolithic Hydrogel. *Analyst* **2012**, *137*, 704−709.
(43) El-Safty, S. A.; Shenashen, M. A.; Ismail, A. A. A Multi-pH-Dependent, Single Optical Mesosensor/Captor Design for Toxic Metals. *Chem. Commun.* **2012**, *48*, 9652−9654.
(44) Khairy, M.; El-Safty, S.; Shenashen, M. A.; Elshehy, E. A. Hierarchical Inorganic−Organic Multi-Shell Nanospheres for Intervention and Treatment of Lead-Contaminated Blood. *Nanoscale* **2013**, *5*, 7920−7927.
(45) Dave, N.; Chan, M. Y.; Huang, P-J. J.; Smith, B. D.; Liu, J. Regenerable DNA-Functionalized Hydrogels for Ultrasensitive, Instrument-Free Mercury(II) Detection and Removal in Water. *J. Am. Chem. Soc.* **2010**, *132*, 12668−12673.
(46) El-Safty, S. A.; Shenashen, M. A. Optical Mesosensor for Capturing of Fe(III) and Hg(II) Ions from Water and Physiological Fluids. *Sens. Actuators, B* **2013**, *183*, 58−70.
(47) Shenashen, M. A.; Elshehy, E. A.; El-Safty, S. A.; Khairy, M. Visual Monitoring and Removal of Divalent Copper, Cadmium, and Mercury Ions from Water by using Mesoporous Cubic Ia3d Aluminosilica Sensors. *Sep. Purif. Technol.* **2013**, *116*, 73−86.
(48) El-Safty, S. A.; Shenashen, M. A.; Ismael, M.; Khairy, M. Mesocylindrical Aluminosilica Monolith Biocaptors for Size-Selective Macromolecule Cargos. *Adv. Funct. Mater.* **2012**, *22*, 3013−3021.
(49) Khairy, M.; El-Safty, S. A.; Ismael, M. Mesoporous Nanomagnet Supercaptors for Selective Heme-Proteins from Human Cells. *Chem. Commun.* **2012**, *48*, 10832−10834.
(50) Ravikovitch, P. I.; Neimark, A. V. Density Functional Theory of Adsorption in Spherical Cavities and Pore Size Characterization of Templated Nanoporous Silicas with Cubic and Three-Dimensional Hexagonal Structures. *Langmuir* **2002**, *18*, 1550−1560.
(51) El-Safty, S. A.; Shahat, A.; Awual, M. R.; Mekawy, M. Large Three-Dimensional Mesocage Pores Tailoring Silica Nanotubes as Membrane Filters: Nanofiltration and Permeation Flux of Proteins. *J. Mater. Chem.* **2011**, *21*, 5593−5603.
(52) Kruk, M.; Hui, C. M. Thermally Induced Transition Between Open and Closed Spherical Pores in Ordered Mesoporous Silicas. *J. Am. Chem. Soc.* **2008**, *130*, 1528−1529.
(53) El-Safty, S.; Mekawy, M.; Yamaguchi, A.; Shahat, A.; Ogawa, K.; Teramae, N. Organic−Inorganic Mesoporous Silica Nanostrands for Ultrafine Filtration of Spherical Nanoparticles. *Chem. Commun.* **2010**, *46*, 3917−3919.
(54) Benoit, J. M.; Mason, R. P.; Gilmour, C. C.; Aiken, G. R. Constants for Mercury Binding by Dissolved Organic Matter Isolates from the Florida Everglades. *Geochim. Cosmochim. Acta* **2001**, *65* (24), 4445−4451.
(55) Ravichandran, M. Interactions between Mercury and Dissolved Organic Matter in the Florida Everglades. Ph.D. Dissertation, University of Colorado, Boulder, CO, 1999.
(56) El-Safty, S. A.; Shahat, A.; Mekawy, M.; Nguyen, H.; Warkocki, W.; Ohnuma, M. Mesoporous Silica Nanotubes Hybrid Membranes for Functional Nanofiltration. *Nanotechnology* **2010**, *21*, 375603.
(57) El-Safty, S.; Shenashen, M. A. Size-Selective Separations of Biological Macromolecules on Mesocylinder Silica Arrays. *Anal. Chim. Acta* **2011**, *694*, 151−161.
(58) El-Safty, S. A. Organic−Inorganic Hybrid Mesoporous Monoliths for Selective Discrimination and Sensitive Removal of Toxic Mercury Ions. *J. Mater. Sci.* **2009**, *44*, 6764−6774.
(59) Liu, J.; Zhao, Z.; Jiang, G. Coating Fe_3O_4 Magnetic Nanoparticles with Humic Acid for High Efficient Removal of Heavy Metals in Water. *Environ. Sci. Technol.* **2008**, *42*, 6949−6954.
(60) Shamsipur, M.; Rajabi, H.; Beyzavi, M.; Sharghi, H. Bulk Polymer Nanoparticles Containing a Tetrakis(3-hydroxyphenyl)-porphyrin for Fast and Highly Selective Separation of Mercury Ions. *Mikrochim. Acta* **2013**, *180*, 791−799.
(61) Aranda, P. R.; Colombo, L.; Perino, E.; De Vito, I. E.; Raba, J. Solid-Phase Preconcentration and Determination of Mercury(II) Using Activated Carbon in Drinking Water by X-ray Fluorescence Spectrometry. *X-ray Spectrom.* **2013**, *42*, 100−104.
(62) Guo, X.; Du, B.; Wei, Q.; Yang, J.; Hu, L.; Yan, L.; Xu, W. Synthesis of Amino Functionalized Magnetic Graphenes Composite Material and Its Application To Remove Cr(VI), Pb(II), Hg(II), Cd(II) and Ni(II) from Contaminated Water. *J. Hazard. Mater.* **2014**, *278*, 211−220.
(63) Zhang, Y.; Yan, L.; Xu, W.; Guo, X.; Cui, L.; Gao, L.; Wei, Q.; Du, B. Adsorption of Pb(II) and Hg(II) from Aqueous Solution Using Magnetic $CoFe_2O_4$-Reduced Graphene Oxide. *J. Mol. Liq.* **2014**, *191*, 177−182.
(64) VanPoecke, R. M. P.; Dicke, M. Signal Transduction Downstream of Salicylic and Jasmonic Acid in Herbivory-Induced Parasitoid Attraction by Arabidopsis Is Independent of JAR1 and NPR1. *Plant, Cell Environ.* **2003**, *26*, 1541−1548.

DOI: 10.1021/acsami.5b02969
ACS Appl. Mater. Interfaces 2015, 7, 13217−13231

(65) Kumari, S.; Chauhan, G. S. New Cellulose "Lysine Schiff-Base-Based Sensor" Adsorbent for Mercury Ions. *ACS Appl. Mater. Interfaces* **2014**, *6*, 5908−5917.
(66) Balaji, T.; El-Safty, S. A.; Matsunaga, H.; Hanaoka, T.; Mizukami, F. Optical Sensors Based on Nanostructured Cage Materials for the Detection of Toxic Metal Ions. *Angew. Chem.* **2006**, *118*, 7360−7366.
(67) Feng, X.; Fryxell, G. E.; Wang, L.-Q.; Kim, A. Y.; Liu, J.; Kemner, K. M. Functionalized Monolayers on Ordered Mesoporous Supports. *Science* **1997**, *276*, 923−926.
(68) El-Safty, S. A.; Ismail, A. A.; Matsunaga, H.; Hanaoka, T.; Mizukami, F. Optical Nanoscale Pool-on-Surface Design for Control Sensing Recognition of Multiple Cations. *Adv. Funct. Mater.* **2008**, *18*, 1485−1500.
(69) Abou-Mesalam, M. M.; Hilala, M. A.; Aridaa, H. A. Environmental Studies on the Use of Synthesized and Natural Ion Exchange Materials in the Treatment of Drinking and Underground Water. *Arab J. Nucl. Sci. Appl.* **2013**, *46*, 63−74.
(70) El-Safty, S. A.; Prabhakaran, D.; Kiyozumi, Y.; Mizukami, F. Nanoscale Membrane Strips for Benign Sensing of Hg(II) Ions: A Route to Commercial Waste Treatments. *Adv. Funct. Mater.* **2008**, *18*, 1739−1750.

DOI: 10.1021/acsami.5b02969
ACS Appl. Mater. Interfaces 2015, 7, 13217−13231